A Lagged Warm Event–Like Response to Peaks in Solar Forcing in the Pacific Region

GERALD A. MEEHL AND JULIE M. ARBLASTER*

National Center for Atmospheric Research,+ Boulder, Colorado

(Manuscript received 7 May 2008, in final form 10 January 2009)

ABSTRACT

The forced response coincident with peaks in the 11-yr decadal solar oscillation (DSO) has been shown to resemble a cold event or La Niña–like pattern during December–February (DJF) in the Pacific region in observations and two global coupled climate models. Previous studies with filtered observational and model data have indicated that there could be a lagged warm event or El Niño–like response following the peaks in the DSO forcing by a few years. Here, observations and two climate model simulations are examined, and it is shown that dynamical coupled processes initiated by the response in the tropical Pacific to peaks in solar forcing produce wind-forced ocean Rossby waves near 5°N and 5°S. These reflect off the western boundary, producing downwelling equatorial Kelvin waves that contribute to transitioning the tropical Pacific to a warm event or El Niño–like pattern that lags the peaks in solar forcing by a few years.

1. Introduction

Previous studies have shown a significant response of earth's climate to variability of solar forcing (e.g., Lean and Rind 2001; Rind 2002; Haigh 2001, 2003; Kuroda and Kodera 2004; van Loon and Shea 2000) and that the responses of the tropical Pacific to peaks of the 11-yr decadal solar oscillation (DSO) resemble cold events, sometimes referred to as La Niña events (van Loon et al. 2004). These are characterized by negative SST anomalies in the equatorial eastern Pacific associated with a strengthening of the climatological precipitation maxima in the intertropical convergence zone (ITCZ) and South Pacific convergence zone (SPCZ) during northern winter and a stronger south Asian monsoon during northern summer (van Loon et al. 2004, 2007). Meehl et al. (2003) first proposed a mechanism that would produce this kind of coupled ocean–atmosphere dynamical response to increasing solar radiation in the first part of the twentieth century. Subsequently, Meehl et al. (2008) have shown this mechanism works for the cold event–like anomalies coincident with peaks in the DSO in two climate model simulations for twentieth-century climate. The question of whether these apparent responses to solar forcing are just coincidentally part of ENSO was addressed by van Loon and Meehl (2008). They showed that the solar response differed from the ENSO signal, particularly in the stratosphere, and the solar-related negative eastern equatorial Pacific SST anomalies persisted for several years around the peaks of the solar forcing, whereas ENSO events more typically last one year.

There is also the possibility that the stratospheric response to solar forcing involving changes in ozone produces comparable effects on the tropics in acting to strengthen the climatological precipitation maxima (Balachandran et al. 1999; Shindell et al. 1999, 2006; Matthes et al. 2006). Thus, the effects from the stratosphere augment and reinforce the coupled response at the surface, as shown by an atmospheric model that resolves stratospheric dynamics and the wavelength dependence of the ozone response from solar forcing coupled into the Community Climate System Model (CCSM) framework (i.e., dynamically coupled to the ocean model, sea ice, and land surface) with a similar La Niña–like response coincident with peaks in the solar forcing (Meehl et al. 2009, manuscript submitted to *Science*).

White et al. (1997) analyzed filtered observations and noted a warm event or El Niño–like response that

* Current affiliation: Bureau of Meteorology, Melbourne, Australia.

+ The National Center for Atmospheric Research is sponsored by the National Science Foundation.

Corresponding author address: Gerald A. Meehl, National Center for Atmospheric Research, P.O. Box 3000, Boulder, CO 80307.
E-mail: meehl@ncar.ucar.edu

DOI: 10.1175/2009JCLI2619.1

lagged the peaks in solar forcing by a few years. A similar signal was documented in a low-resolution climate model run with an idealized 11-yr solar forcing (White and Liu 2008a). At first inspection, it was thought that this was a fundamentally different type of response to solar forcing compared to the earlier Meehl et al. (2003, 2008) works and could be in contradiction with these works. However, the lagged warm event signal relative to the initial cold event signal suggests dynamical coupled processes produced initially, which could subsequently cause a lagged warm event response. We explore this possibility in this paper with observations and two global coupled climate model simulations. We will present evidence to indicate that this is indeed the case, showing how dynamical coupled processes in the tropical Pacific can respond to external forcing in a similar way to internally generated ENSO variability.

2. Observed data and models

The observed data used in our study are the Hadley Centre Sea Ice and Sea Surface Temperature (HadISST) reconstructed dataset from 1890 to 2006 (Rayner et al. 2003). Additional observed SST data come from the Simple Ocean Data Assimilation (SODA) ocean reanalysis product (Carton et al. 2000; for the period 1958–2004) along with upper-ocean temperatures. From those, we compute upper-ocean heat content as the integral of layer temperatures over the upper 150 m of the ocean. The wind stress forcing data from the SODA reanalayses are used to compute wind stress curl. Composites from HadISST are formed for peak solar years as in van Loon et al. (2007), with the January year 0 (Jan 0) designated for 12 peak solar years: 1883, 1893, 1905, 1917, 1928, 1937, 1947, 1957, 1968, 1979, 1989, and 2000. For the SODA data with the shorter record, composites are formed from the last four peak solar years.

Output from two global coupled climate models is analyzed in this paper. The Parallel Climate Model (PCM), first described by Washington et al. (2000), has been used for numerous climate studies and, as noted above, was used in the study by Meehl et al. (2008). The resolution of the atmosphere is T42, or roughly 2.8° × 2.8°, with 18 levels in the vertical, the majority of which are in the troposphere (model layer midpoints: 4.8, 13.1, 32.6, 63.9, 99.0, 138.7, 189.2, 251.2, 324.8, 409.0, 501.3, 598.2, 695.2, 786.5, 866.4, 929.3, 970.4, and 992.5 hPa). Resolution in the ocean is roughly ⅔° tapering down to ½° in the equatorial tropics, with 32 levels. No flux adjustments are used in the model. The interannual climate variability related to ENSO is in good agreement with observations (Meehl et al. 2001; Dai et al. 2001). The amplitude of El Niño events in PCM is close to observed, but the frequency is in the 3–4-yr range as opposed to observations that show more of a 3–7-yr spectral peak (Meehl et al. 2006a).

We analyze four-member ensembles of twentieth-century climate that branched from a preindustrial control run. In this ensemble of opportunity (the largest number that could be run with available computer resources), the signals from solar forcing are composites centered around peak years in solar forcing as in van Loon et al. (2007). The simulations use combinations of observed anthropogenic and natural forcings, including greenhouse gases (GHGs), the direct effect of sulfate aerosols, tropospheric and stratospheric ozone, solar variability, and volcanoes (Meehl et al. 2004). Reconstructions of total solar irradiance for PCM and CCSM, version 3 (CCSM3) are from Hoyt and Schatten (1993) and Lean et al. (1995), respectively. The time series were updated from the original sources up to 1999 (T. Wigley, NCAR, 2009, personal communication with P. Foukal and C. Frohlich). The reconstructions are a bit different from each other, so the years for peak solar forcing in each had to be accounted for in calculating the composites. The important aspect for the model response is analyzing the signal from the peak solar forcing years in the respective forcing datasets. The twentieth-century simulations were started at intervals of roughly 10–20 yr from a long control run with constant preindustrial conditions for the year 1870 (the same technique was used for the CCSM3 below). A four-member ensemble with only the solar forcing included (Meehl et al. 2004) shows a similar response to the full set of forcings (not shown).

The CCSM3 is described by Collins et al. (2006). The twentieth-century simulations analyzed here are from the T85 version of CCSM3, with the Community Atmospheric Model, version 3 (CAM3) as the atmospheric model component. Grid points in the atmosphere are spaced roughly every 1.4° latitude and longitude, and there are 26 levels in the vertical with a majority of the levels in the troposphere (model layer midpoints: 3.5, 7.4, 14.0, 23.9, 37.2, 53.1, 70.1, 85.4, 100.5, 118.3, 139.1, 163.7, 192.5, 226.5, 266.5, 313.5, 368.8, 433.9, 510.5, 600.5, 696.8, 787.7, 867.2, 929.6, 970.6, and 992.6 hPa). The ocean is a version of the Parallel Ocean Program (POP) with a nominal latitude–longitude resolution of 1° (½° in the equatorial tropics) and 40 levels in the vertical. No flux adjustments are used in the CCSM3.

A five-member ensemble of CCSM3 twentieth-century simulations is analyzed here. The twentieth-century simulations were started from different times in the 1870 control run separated by 20 yr with the first ensemble member branching from the control run at year 360. The natural and anthropogenic forcings are

described in Meehl et al. (2006b), and the solar forcing in CCSM3 is the Lean et al. (1995) total solar irradiance (TSI) reconstruction. ENSO variability is very biennial in this model (Deser et al. 2006).

The response to the two different solar forcing datasets was shown by Meehl et al. (2006b). The differences between the two lie in the time evolution of the multidecadal variability of the solar forcing. Hoyt and Schatten (1993) show an earlier multidecadal peak of the solar forcing in the mid-1940s, whereas Lean et al. (1995) show a somewhat later peak in the 1950s. The DSO forcing is comparable between the two.

3. The SST response to solar forcing in the tropical Pacific

As noted above, van Loon et al. (2007) documented a La Niña– or cold event–like response to peaks in the DSO for northern winter. Meehl et al. (2008) followed that study with an analysis of two climate model simulations (CCSM3 and PCM) that produced a similar response to that seen in the observations. They also described a possible mechanism to account for this response, which followed from the Meehl et al. (2003) study that first proposed such a dynamically coupled mechanism at the surface that could be initiated by increased solar forcing.

Meehl et al. (2008) noted the amplitude of the SST response in the models in the tropical Pacific is about half the magnitude of the observations. These models have poorly resolved stratospheres and no 11-yr ozone variations, so the mechanism depends almost entirely on the increased solar forcing at peaks in the DSO acting on the ocean surface in clear-sky areas of the equatorial and subtropical Pacific. This solar forcing can be greater in those regions by about a factor of 2 than the globally averaged solar forcing if clouds do not change in the specific locations being examined (Lean et al. 2005). This number is calculated by taking the globally averaged top-of-atmosphere incident solar radiation and dividing by 4 to take into account the curvature of the earth, and another factor of about 0.7 to take into account albedo, which amounts to about a factor of 6 (Lean et al. 2005). At the surface at a given location, the diurnal cycle must be taken into account (dividing by π), thus producing about a factor of 2 greater than the global average at a given location. However, looking at the differences in net solar radiation at the surface in certain locations, this number is higher because of cloud feedbacks.

The mechanism involves the increased solar forcing at the surface being manifested by increased latent heat flux and evaporation. The resulting moisture is carried to the convergence zones by the southeast (SE) trades, thereby strengthening the ITCZ and SPCZ. Once these precipitation regimes begin to intensify, an amplifying set of coupled feedbacks similar to that in cold events (or La Niña events) occurs. There is a strengthening of the SE trades and greater upwelling of colder water that extends the equatorial cold tongue farther west and reduces precipitation across the equatorial Pacific while increasing precipitation even more in the ITCZ and SPCZ. The large-scale north–south (Hadley) and east–west (Walker) circulations strengthen and intensify subsidence in the north and south Pacific subtropical highs to further reduce clouds there and enhance even more the increase of solar forcing in those regions. These cloud feedbacks are important to amplify the solar forcing at the surface.

Regarding the part of the mechanism that involves an intensification of the Hadley and Walker circulations, van Loon and Labitzke (1994) analyzed observations and showed that the Hadley circulation was strengthened in solar maximum years. Gleisner and Thejll (2003) documented a poleward expansion of the Hadley circulation in peak solar years in observations, with stronger ascending motions at the edge of the rising branch, as well as a stronger Walker circulation with enhanced upward motion in the tropical western Pacific connected to stronger descending motions in the tropical eastern Pacific. Both Kodera (2004) and van Loon et al. (2004) examined observations of the Indian monsoon and found evidence for enhanced summer-season off-equatorial monsoon precipitation over India. Other studies have shown that stronger summer monsoon precipitation implies a stronger large-scale east–west (or Walker) circulation (e.g., Meehl 1987).

Evidence for a consistent change of the Hadley and Walker circulations in peak solar years from modeling studies is more mixed, perhaps because of a number of model simulations being run with specified SSTs and a noninteractive ocean. For example, using a model with specified SSTs, Haigh et al. (2005) documented weakened Hadley cells for peak solar years but with a poleward expansion. This poleward expansion was seen in the observations in van Loon et al. (2007) and was noted to be important for the dynamically coupled response to solar forcing by Meehl et al. (2008), using observations and two global coupled models with interactive ocean components. Matthes et al. (2006) showed a poleward shift of the precipitation maximum in the tropical western Pacific by using a model with prescribed SSTs, and Balachandran et al. (1999), also using a model with specified SSTs, saw a strengthening of the off-equatorial climatological precipitation maxima coincident with peak solar forcing. Shindell et al. (2006), using a global

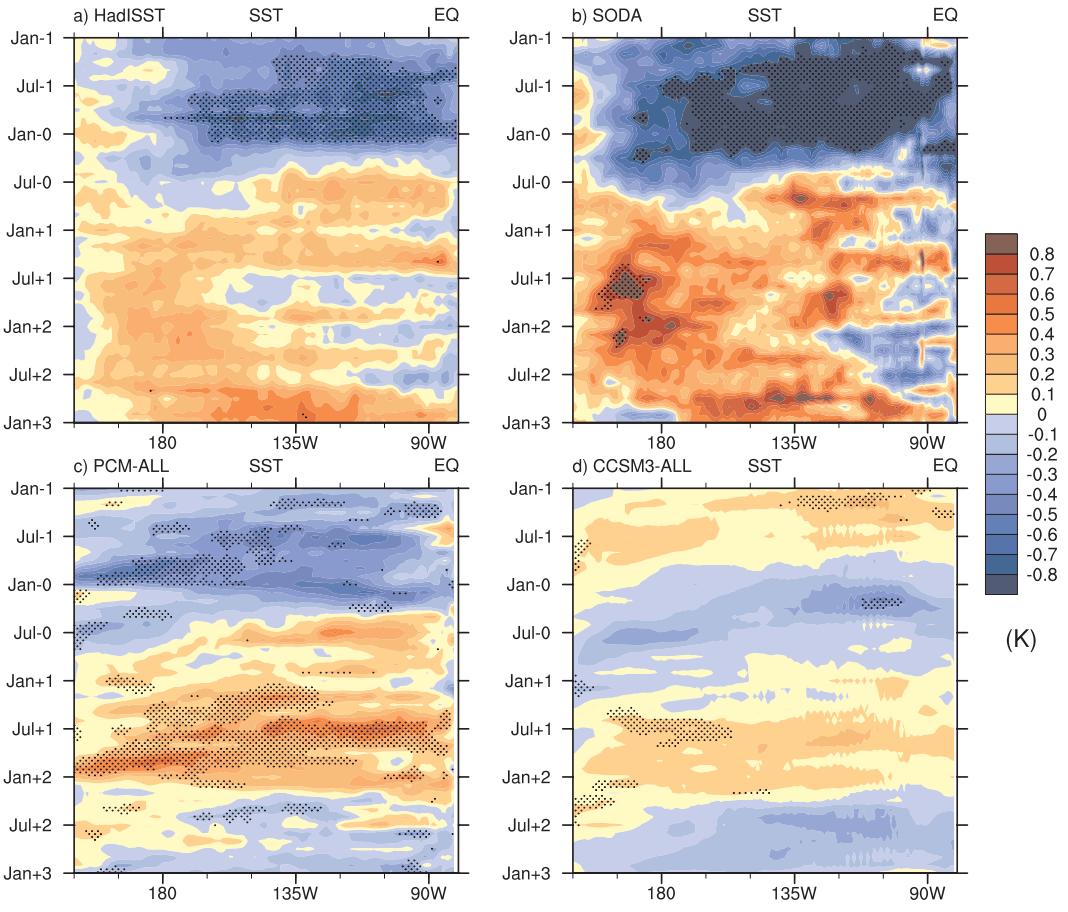

FIG. 1. Hovmöller diagrams of composite SST differences, peak solar years (year 0), the year before (year −1), and the three years following the peak solar years (years +1, +2, and +3), minus climatology for the twentieth century (a) observed from the HadISST data, (b) observed from the SODA ocean reanalysis, (c) composite of four model simulations with PCM, and (d) composite of five model simulations with CCSM3. Stippling in (a),(b) indicates the 90% significance level from a *t* test. Units are on the color bar, and stippling in (c),(d) indicates that the mean signal divided by the interensemble standard deviation exceeds one.

coupled model, documented enhanced climatological precipitation maxima in the tropics for peak solar forcing. Therefore, the predominance of published evidence is consistent with the notion that peaks in solar forcing are associated with enhanced upward motion and precipitation in the climatological tropical precipitation maxima.

Through similar reasoning, this mechanism should produce the opposite-sign anomalies forced by large tropical volcanic eruptions (e.g., Mann et al. 2005). Preliminary model results show this response indeed occurs and this will be the subject of a subsequent paper.

Van Loon and Meehl (2008) showed that the cold event–like response was not confined only to the years of the peak solar forcing but also extended to parts of the previous and following years. This is seen in Hovmöller diagrams along the equator of observed SSTs from the HadISST and SODA data (Figs. 1a,b). There are consistent negative SST anomalies for the year of the peak in solar forcing in these composites centered on Jan 0. However, these negative SST anomalies are already present the year before (Jan −1, "−1" refers to the year before peak solar) and extend to early in year +1 near the international date line.

However, it is notable that both observational datasets show a transition to warm event–like conditions starting late in year 0, with these positive SST anomalies in the equatorial Pacific persisting for the next two years or so (Figs. 1a,b).

Comparing the two models (Figs. 1c,d), the PCM shows a stronger signal than CCSM3 and is also closer to the observations, but the timing is somewhat different between the models and observations. In PCM, the negative SST anomalies are present in Jan −1, as in the observations, and persist near the date line until late in year 0. And, as in the observations, PCM shows positive

SST anomalies that appear in year 0. But unlike the observations, these positive SST anomalies only persist until midyear +1. CCSM3 has the weakest signal, with negative SST anomalies appearing in the eastern equatorial Pacific late in year −1 and then persisting only through most of year 0. The transition to positive SST anomalies occurs early in year +1 and then returns to negative SST anomalies in midyear +2.

The character of the response of the observations and models is consistent with the time scales of ENSO variability. As noted above, PCM has ENSO frequencies of 3–4 yr, whereas CCSM3 is very biennial. The response to solar forcing reflects those preferred frequencies of equatorial Pacific SST variability, with PCM transitioning from cold to warm and back to cold states. Thus, the models' response to solar reflects their ENSO tendencies. Their largest La Niña–like response is timed to the peak in solar forcing, even though there is a multiyear period of maximum solar forcing. Thus, their dynamical response (and to a certain extent in the observations as well) overcomes the solar forcing that would tend to produce ongoing La Niña–like signals and the system transitions to an El Niño–like state. So, the observations and models are stimulated most effectively around the peak solar forcing year, and their respective time scales of dynamical response dictate the evolution of how the coupled system evolves in response to that forcing.

To illustrate the spatial character of the transition from a cold event–like to a warm event–like pattern, Figs. 2–4 show SST anomalies for the peak solar year composites for the December–February (DJF) 0, DJF +1, and DJF +2 seasons. As noted in van Loon and Meehl (2008), there is still some remnant of the cold event pattern in DJF +1 but positive SST anomalies have appeared near the international date line. This pattern persists to DJF +2 in Fig. 2c. For the PCM in Fig. 3, the cold event–like pattern in Fig. 3a gives way to a warm event–like pattern already in DJF +1 (Fig. 3b). That pattern then strengthens in DJF +2 (Fig. 3c). For CCSM3 in Fig. 4, the cold event–like pattern in DJF 0 becomes a weak warm event pattern in DJF +1 that is stronger in DJF +2.

4. Dynamical coupled response in the Pacific region

As noted in the introduction, we hypothesize that the solar forcing produces a cold event–like response centered on the peak year of solar forcing that then initiates dynamically coupled processes involving wind-forced off-equatorial ocean Rossby waves. As in the delayed-action oscillator mechanism (e.g., White et al. 2003), these produce a transition from cold event to warm event conditions. This would involve negative wind stress curl anomalies near 5°N and 5°S that would force the downwelling Rossby waves with associated positive heat content anomalies. The ocean Rossby waves near these latitudes would have propagation speeds of around 0.35 m s^{-1}, so that they would reach the western boundary in about a year, reflect into the equatorial waveguide, and produce downwelling Kelvin waves. These would deepen the thermocline, reduce upwelling of cool water, and result in a transition from negative to positive SST anomalies with a lag of 1–2 yr.

To investigate this possibility in observations and the models, Figs. 5, 6, and 7 show Hovmöller diagrams of composite zonal wind stress and heat content anomalies for different latitudes in the Pacific. First, for the observations, Figs. 5a–c show composite zonal wind stress anomalies, peak years minus climatology, from the SODA data. For the northern winter of the peaks in solar forcing (Jan 0), there are easterly wind stress anomalies (negative values) at the equator from about 130°W westward to the western Pacific (Fig. 5b) associated with negative SST anomalies across almost the entire equatorial Pacific (Fig. 1a). Meehl et al. (2008) describe the intensification of the precipitation maxima in the Pacific region that then intensify the Hadley and Walker circulations, thus producing this strengthening of the trade winds. Also during Jan 0, there are negative upper-ocean heat content anomalies from the date line eastward (Fig. 5e). However, at that time, some positive heat content anomalies in the equatorial western Pacific (Fig. 5e) associated with westward propagating positive heat content anomalies at 5°N (Fig. 5d) and 5°S (Fig. 5f, highlighted by solid black lines slanting downward from right to left) formed near the date line nearly a year before (Jan −1). These are propagating at about 0.35–0.45 m s^{-1}, or the theoretical phase speed of mode-1 ocean Rossby waves near 5°–10°N (e.g., White et al. 2003). These positive heat content anomalies can be traced back across the Pacific to the east to near the date line.

It was noted in Meehl et al. (2008) that the ITCZ and SPCZ strengthen and shift somewhat poleward in association with the stronger equatorial Pacific cold tongue as in observed La Niña events. This poleward shift is important because near 10°N and 10°S, the convergence zone lies in areas that normally see strong trade winds flowing into the convergence zones just equatorward. Because there are very light winds in the convergence zones, the net effect is to produce westerly wind stress anomalies near 10°N and 10°S in the observations (Figs. 5a,c) that are evident in Jan −1 near 135°W but are readily apparent by July (Jul) −1, near the date line, particularly near 10°N. Thus, the positive zonal wind stress anomalies near 10°N and 10°S and

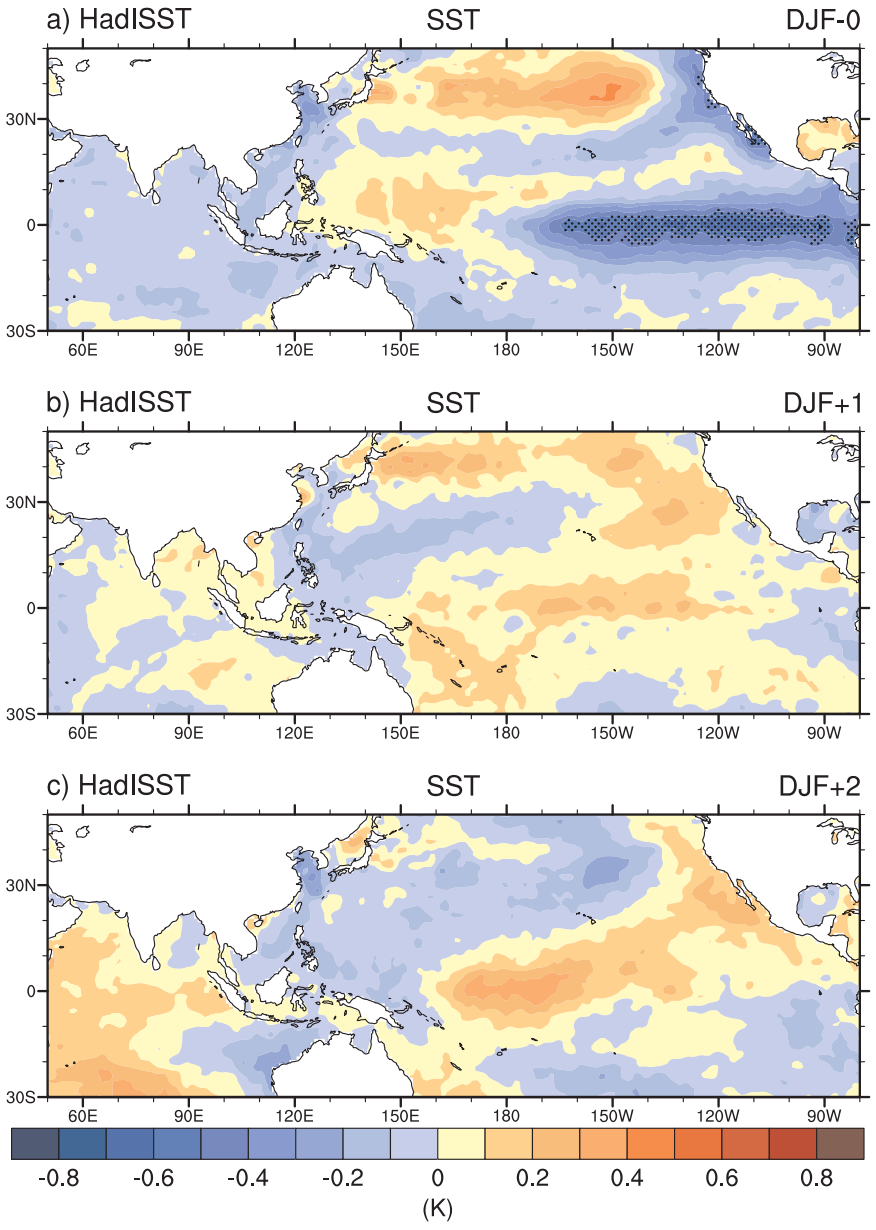

FIG. 2. Composite SST differences for DJF season minus climatology for (a) peak solar years (DJF 0), (b) DJF +1, and (c) DJF +2. Units are on the color bar and stippling indicates the 90% significance level from a *t* test.

negative zonal wind stress anomalies near the equator produce anomalous wind stress gradients between the equator and 10°N and 10°S, and this should set up negative wind stress curl anomalies near 5°N and 5°S.

Indeed, mostly negative wind stress curl anomalies near 5°N and 5°S are evident by Jul −1 and are more extensively established in Jan 0 (Figs. 8a,b, respectively). These negative wind stress curl anomalies force downwelling ocean Rossby waves with a signature of positive heat content anomalies in Figs. 5d,f that propagate westward. Evidence of their reflection off the western boundary and into the equatorial waveguide can be seen as downwelling Kelvin waves (the positive heat content anomalies in the equatorial western Pacific in Fig. 5e, highlighted by the solid black line slanting downward from left to right) that successively propagate farther eastward until by Jul 0 there are positive equatorial heat content anomalies and a deeper equatorial thermocline right across the equatorial Pacific. It is at this time in Figs. 1a,b that the SST anomalies begin

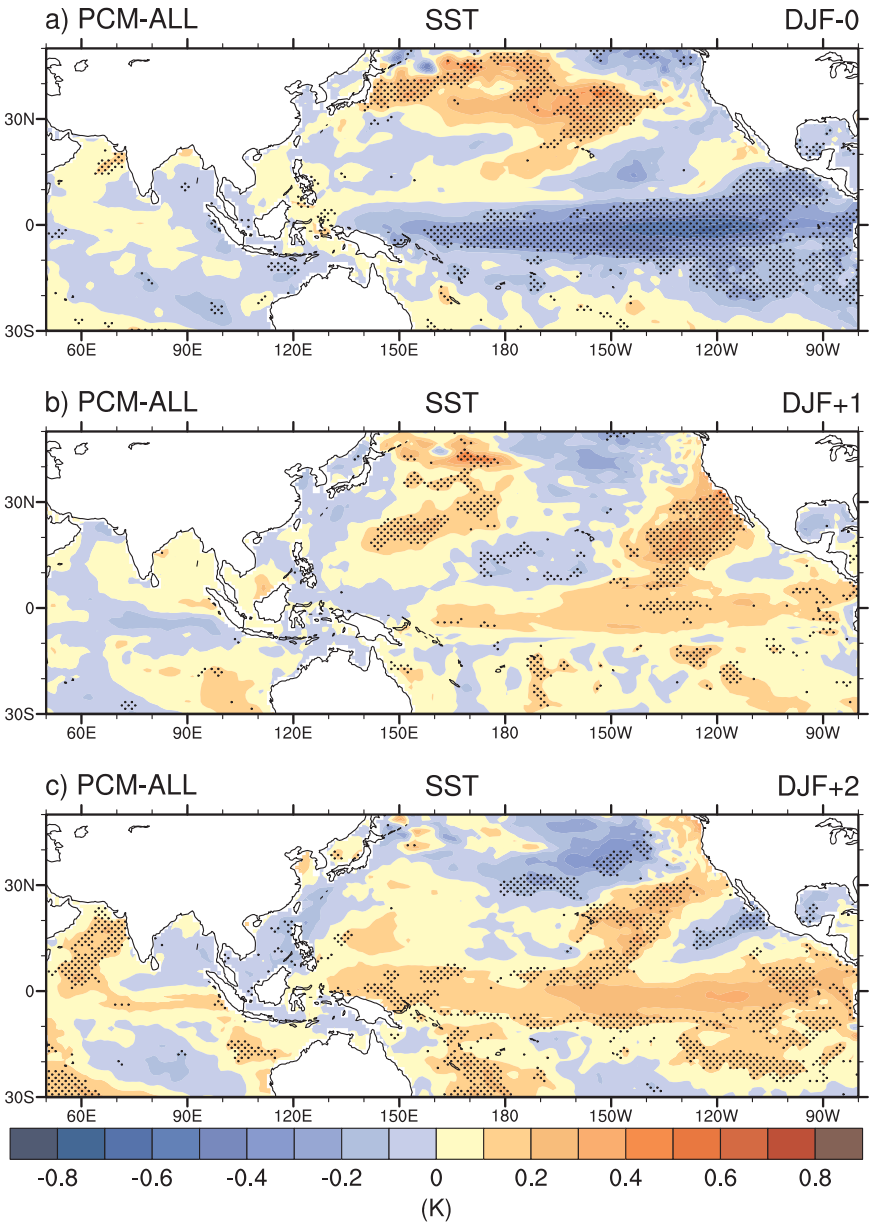

FIG. 3. Composite SST differences from a four-member ensemble mean from PCM for DJF season minus climatology for (a) DJF 0, (b) DJF +1, and (c) DJF +2. Units are on the color bar and stippling indicates that the composite difference exceeds one interensemble standard deviation.

to transition from negative to positive. The deeper equatorial thermocline would be associated with upwelling of warmer water, thus contributing to the change of sign of equorial SSTs from negative to positive. By Jan +1, there are mostly positive SST anomalies across the Pacific in Figs. 1a,b and 2b. The positive SST and heat content anomalies are evident with fluctuating amplitude for the next two years or so (Figs. 1a,b, and 2c).

Thus, the transition from cold event–like conditions in the equatorial Pacific in Jul −1 and Jan 0 to warm event–like anomalies in Jan +1 and Jan +2 involves wind-forced ocean Rossby waves near 5°N and 5°S that propagate westward, reflect at the western boundary, come back across the equatorial Pacific as downwelling Kelvin waves that deepen the thermocline (increased heat content anomalies), and contribute to a transition from negative to positive SST anomalies

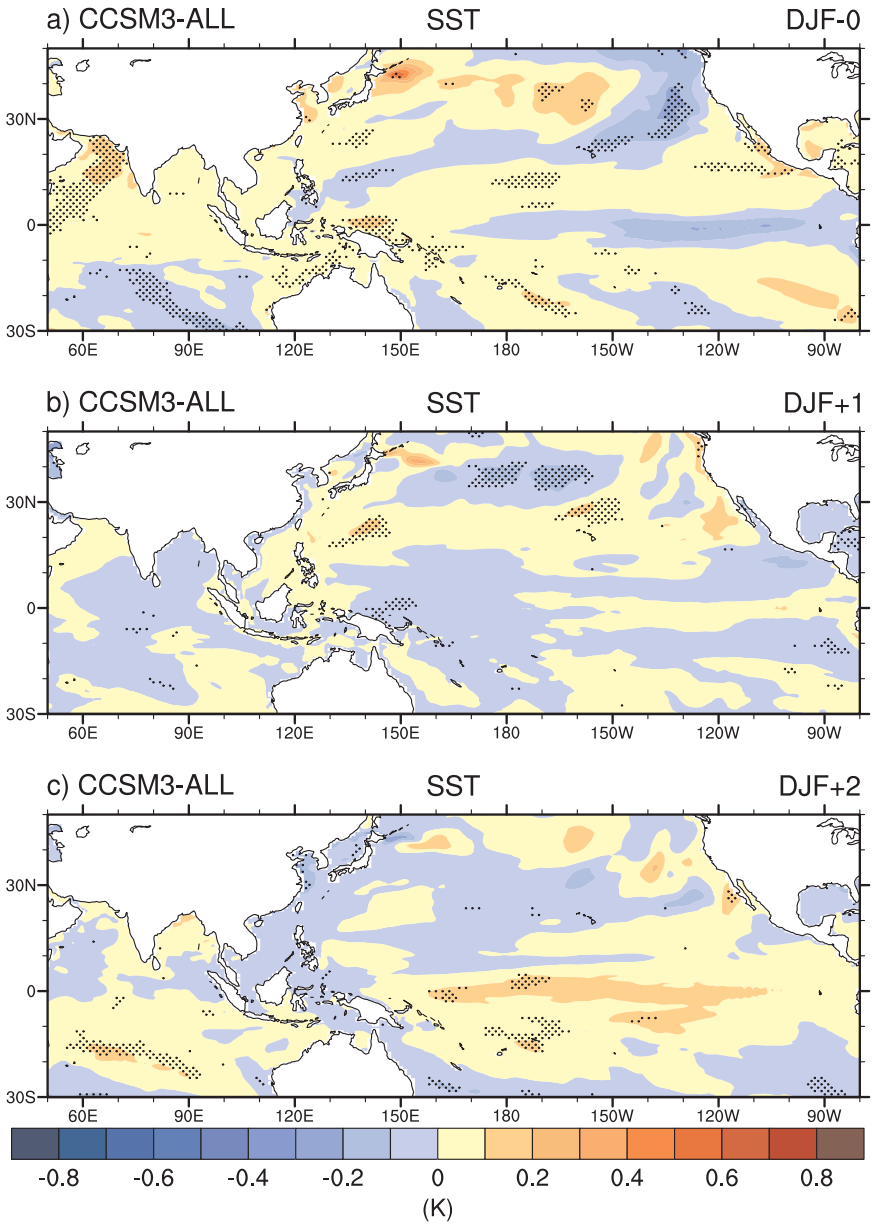

FIG. 4. Composite SST differences from a five-member ensemble mean from CCSM3 for DJF season minus climatology for (a) DJF 0, (b) DJF +1, and (c) DJF +2. Units are on the color bar and stippling indicates that the composite difference exceeds one interensemble standard deviation.

with a lag of a few years from the peak years of solar forcing.

For the PCM and CCSM3, similar Hovmöller diagrams to those for the observations are shown in Figs. 6 and 7, respectively. As in the observations in Fig. 5b, there are negative zonal wind stress anomalies in PCM at the equator from about 130°W westward past the international date line present in Jan −1 and lasting until about Jul 0 (Fig. 6b). CCSM3 has equatorial Pacific negative zonal wind stress anomalies for a shorter duration than the observations or PCM, lasting only from about Jul −1 to Jul 0 (Fig. 7b). The positive zonal wind stress anomalies near 10°N and 10°S, noted for the observations in Figs. 5a,c, are seen in PCM as well, particularly near 10°N early in year 0 in Fig. 6a, with some similar but weaker anomalies near 10°S in Fig. 6c. CCSM3 also shows evidence of positive zonal wind stress anomalies in Jan 0 in the eastern and western

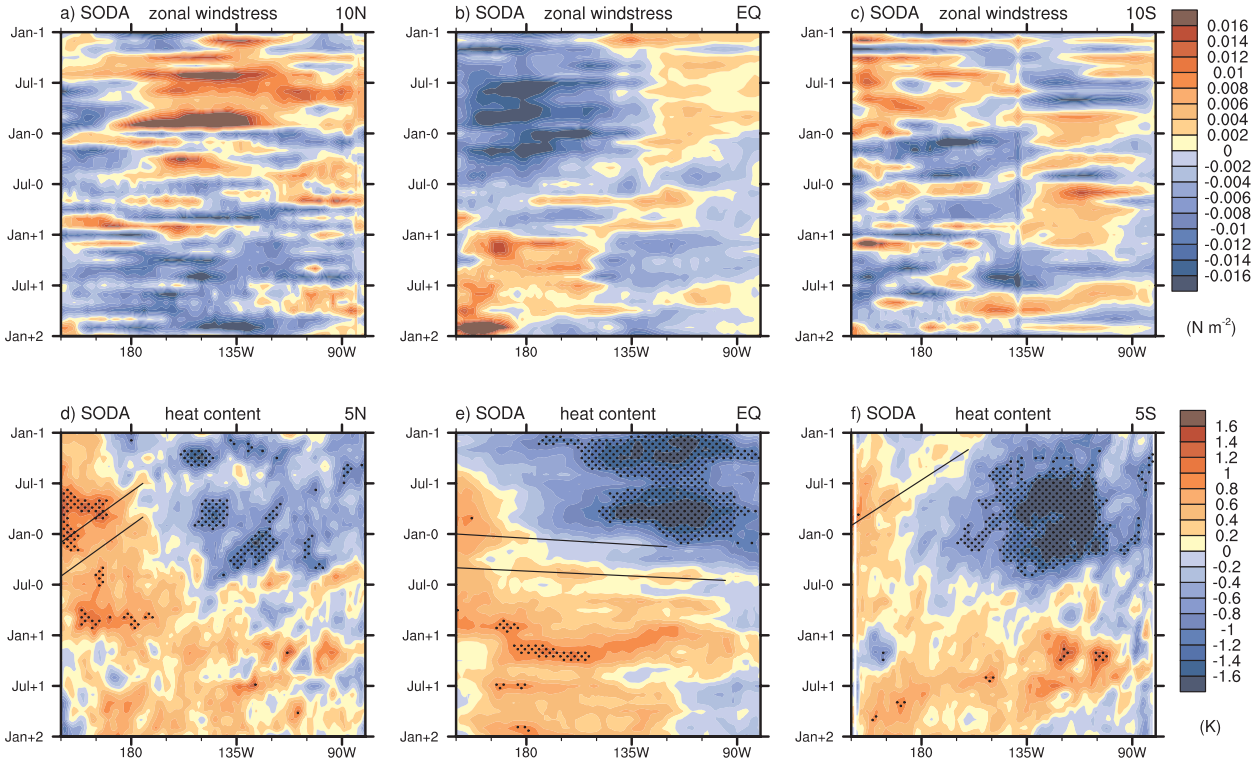

FIG. 5. Composite differences for peak solar years (year 0) minus climatology from the SODA ocean reanalysis data, as well as years −1, +1, and +2 for (a) zonal wind stress at 10°N, (b) zonal wind stress at the equator, (c) zonal wind stress at 10°S, (d) upper-ocean heat content at 5°N, (e) upper-ocean heat content at the equator, and (f) upper-ocean heat content at 5°S. Units are on the color bar and stippling indicates significance at the 90% level from a *t* test. Solid lines highlight ocean Rossby waves (slanting down from right to left) and equatorial Kelvin waves (slanting down from left to right).

Pacific near 10°N (Fig. 7a), with weaker anomalies near 10°S (Fig. 7c). Such zonal wind stress anomalies in the observations, with positive anomalies near 10°N and 10°S and negative values near the equator, were shown to produce negative wind stress curl anomalies in Figs. 8a,b. Similar anomalies are seen for PCM in Figs. 8c,d and CCSM3 in Figs. 8e,f. These negative wind stress curl anomalies near 5°N and 5°S are particularly prominent in Jan 0 (Figs. 8d,f). As a consequence, downwelling Rossby waves are initiated near 5°N and 5°S, as in the observations and evidenced by westward propagating positive heat content anomalies in the PCM (Figs. 6d,f) and CCSM3 (Figs. 7d,f) that are prominent in Jan 0 arriving at the western boundary. These reflect as downwelling equatorial Kelvin waves (positive eastward propagating heat content anomalies) in year 0 for both models (Figs. 6e, 7e), which are also seen in the observations in Fig. 5e, with stronger signals in PCM in Fig. 6. These Kelvin waves contribute to deepening the thermocline and as in the observations in Figs. 1a,b produce a transition to positive SST anomalies late in year 0 and into year +1 in the models (Figs. 1c,d).

The persistence of the positive equatorial SST anomalies for a few years after the peak in solar forcing seen in the observations in Figs. 1b,c is not as distinct in the models, in which both have transitioned back to negative equatorial heat content anomalies in the first half of year +2 (Figs. 6e, 7e), whereas the observations maintain mostly positive equatorial heat content (Fig. 5e) and SST anomalies (Figs. 1a,b) out to year +3. The more rapid transitions seen in both models are related to their shorter ENSO periods noted earlier. Thus, when solar forcing produces cold event–like conditions, the coupled dynamics of the models tend toward shorter periods and a more rapid transition back from warm event conditions a year or two after the peak in solar forcing.

5. Discussion and concluding remarks

Earlier studies documented a La Niña– or cold event–like response in the tropical Pacific that is coincident with peaks in the 11-yr solar forcing cycle. Other studies noted an El Niño– or warm event–like response in the tropical Pacific lagging peaks in solar forcing by a few

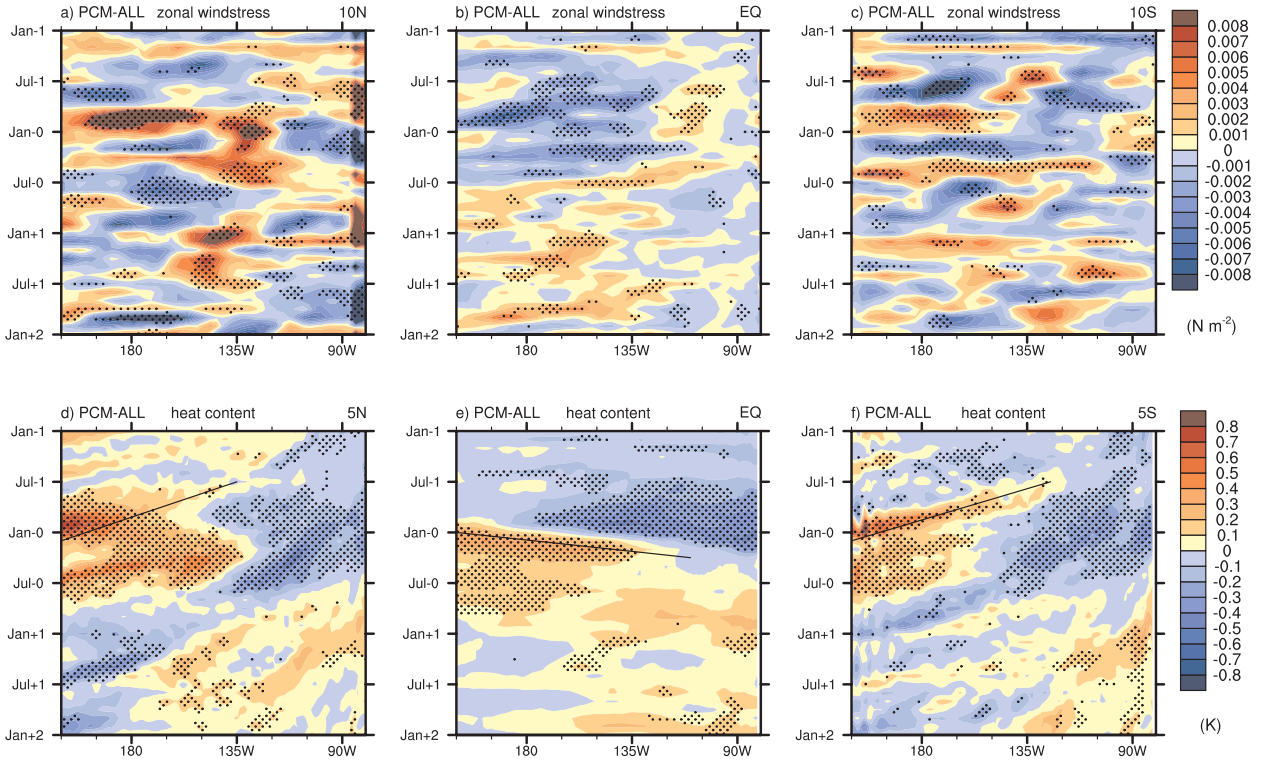

FIG. 6. As in Fig. 5, but for the ensemble mean PCM experiments and stippling indicates that the composite difference exceeds one interensemble standard deviation.

years. Here, we use observations and results from two global coupled climate models to show that these processes are not inconsistent but, in fact, follow from the coupled dynamics of the tropical Pacific. The initial cold event response produces negative wind stress curl anomalies near 5°N and 5°S in observations and models that then force westward propagating downwelling ocean Rossby waves. They reflect at the western boundary and produce eastward-propagating downwelling Kelvin waves in the equatorial Pacific. Their positive heat content anomaly signatures represent a deeper thermocline, and a warming of equatorial Pacific SSTs follows with a lag of about 1–2 yr. The horizontal resolutions in the two models in this paper are different, although both show a qualitatively similar response, which suggests that resolution is not the most important factor in reproducing this oceanic wave effect.

These dynamically coupled processes, prompted by forcing from the sun, are then consistent between the cold event–like response coincident with peaks in the DSO documented by van Loon et al. (2007) and the lagged warm event–like response to peaks in the DSO noted by White et al. (1997) and White and Liu (2008a). White and Liu (2008b) take this argument one step further and postulate that nonlinear phase locking of the third and fifth harmonics is initiated from the solar-forced first harmonic with an 11-yr period, thus explaining about 52% of the interannual variance in the Niño-3 area-averaged eastern equatorial Pacific SST index from 1900 to 2005.

A related idea arises from the fact that the spectrum of the time series of solar forcing has both an 11-yr peak and interannual peaks [Hoyt and Schatten 1997—also seen in an multitaper method (MTM) spectrum computed from the solar forcing used in the models; not shown], which possibly could be forcing the interannual response of Niño-3.4 (area-averaged SSTs in the tropical eastern Pacific from 5°N to 5°S and from 170° to 120°W) in the models (also seen in the MTM spectra of the Niño-3.4 time series from observations, the ensemble means of the two forced model experiments, and the two unforced model control runs; not shown). As noted earlier, such interannual peaks in the spectrum of solar forcing arise from the nonsinusoidal nature of the DSO (steep rise and fall punctuated by several years near either the solar maximum or minimum), along with year-to-year variations of the solar forcing values (Lean et al. 2005).

To further quantify the connection between solar forcing and tropical Pacific SST variability with roughly an 11-yr frequency, the MTM/singular value decomposition (SVD) methodology (Mann and Park 1999; used, e.g., by White and Tourre 2003; Tourre and White 2006)

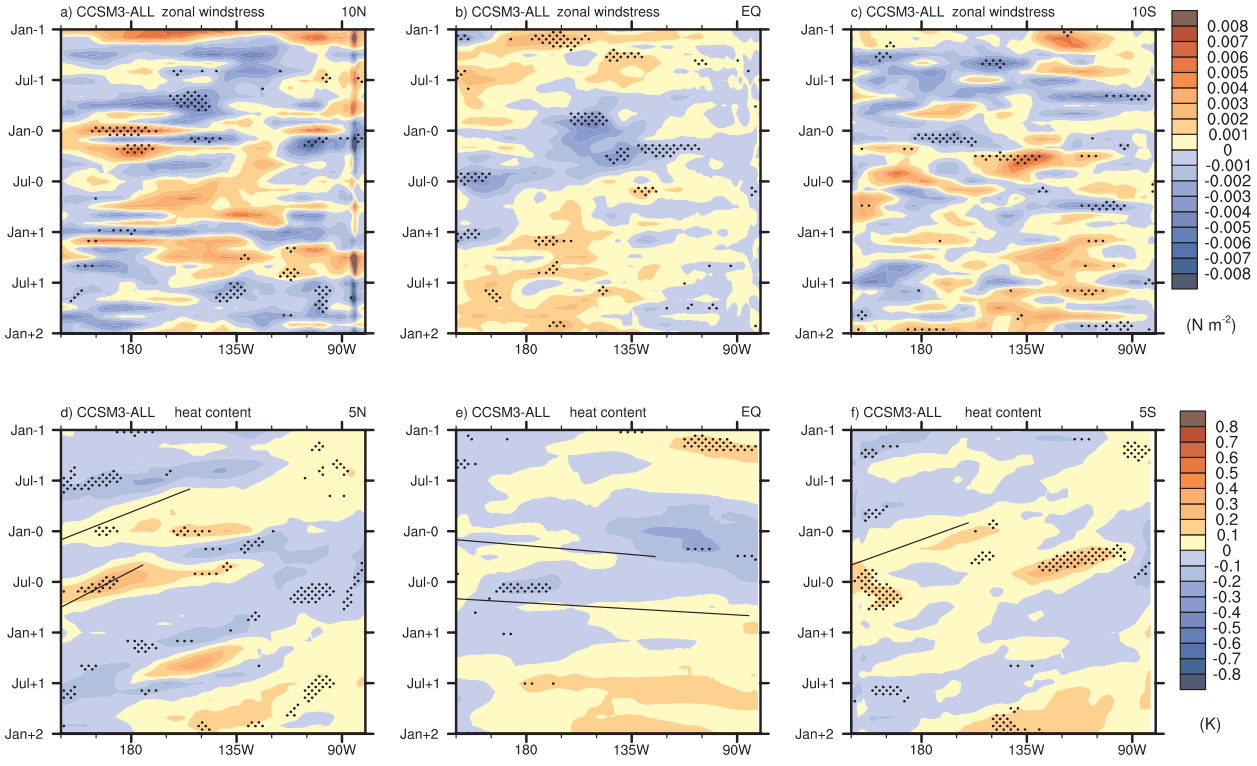

FIG. 7. As in Fig. 5, but for the five-member ensemble mean CCSM3 experiments and stippling indicates that the composite difference exceeds one interensemble standard deviation.

is first applied to time series of Niño-3.4 from the CCSM3 preindustrial control run and solar forcing (Lean et al. 1995) and then to time series of Niño-3.4 from the ensemble average of CCSM3 twentieth-century all-forcings runs and the Lean et al. (1995) solar forcing using the SSA-MTM toolkit (Ghil et al. 2002; Dettinger et al. 1995, especially 12–14, 21). For the control run in Fig. 9a, because there is no solar forcing included in that model simulation, any significant peaks would occur by coincidence. Thus, there is no significant peak near 11 yr, which indicates that there is little coincident covariability between the 11-yr solar forcing and variability at that time scale in the control run Niño-3.4 time series. The only significant coincidental peaks occur for frequencies less than three years, and these arise from small amplitude biennial variability in the solar forcing spectra (not shown) and significant biennial variability in the CCSM3 Niño-3.4 time series (noted earlier). For the all-forcings ensemble mean in Fig. 9b, there is a peak near 11 yr, significant at the 99% level, indicating that the 11-yr peak in the solar forcing time series spectra (not shown) forces covariability at 11 yr in the twentieth-century ensemble mean spectra, which includes solar forcing. The other significant peaks occur at frequencies less than three years, which were shown to be coincidental from the control run in Fig. 9a. Therefore, there is a significant response at frequencies around 11 yr, which shows covariability between the solar forcing and the Niño-3.4 response.

To quantify the significance of a forced negative Niño-3.4 signal coincident with peaks in solar forcing followed by a positive Niño-3.4 value two years later, we computed 90% and 95% confidence intervals using a distribution of averages from the long control runs of the models. To create the distribution, $11 \times N$ randomly chosen values of Niño-3.4 DJF SSTs were averaged to mimic the averaging over 11 solar maxima and N ensemble members of the twentieth-century simulations, repeated 500 times. The resulting 90% and 95% confidence intervals, along with the forced signals for the observations and twentieth-century simulations, show that the combination of negative Niño-3.4 coincident with peak solar years, followed two years later by a positive value of Niño-3.4, is significant for the observations at the 90% level for the peak solar years (Niño-3.4 = −0.48°C) and at the 95% significance level for the 2-yr lag (Niño-3.4 = +0.62°C), using the CCSM3 control to derive the significance levels. The PCM negative–positive sequence was significant at the 95% level for both time periods (Niño-3.4 = −0.30° and +0.48°C), whereas the CCSM3, though having the correct negative–positive sequence, was not significant at the 90% level

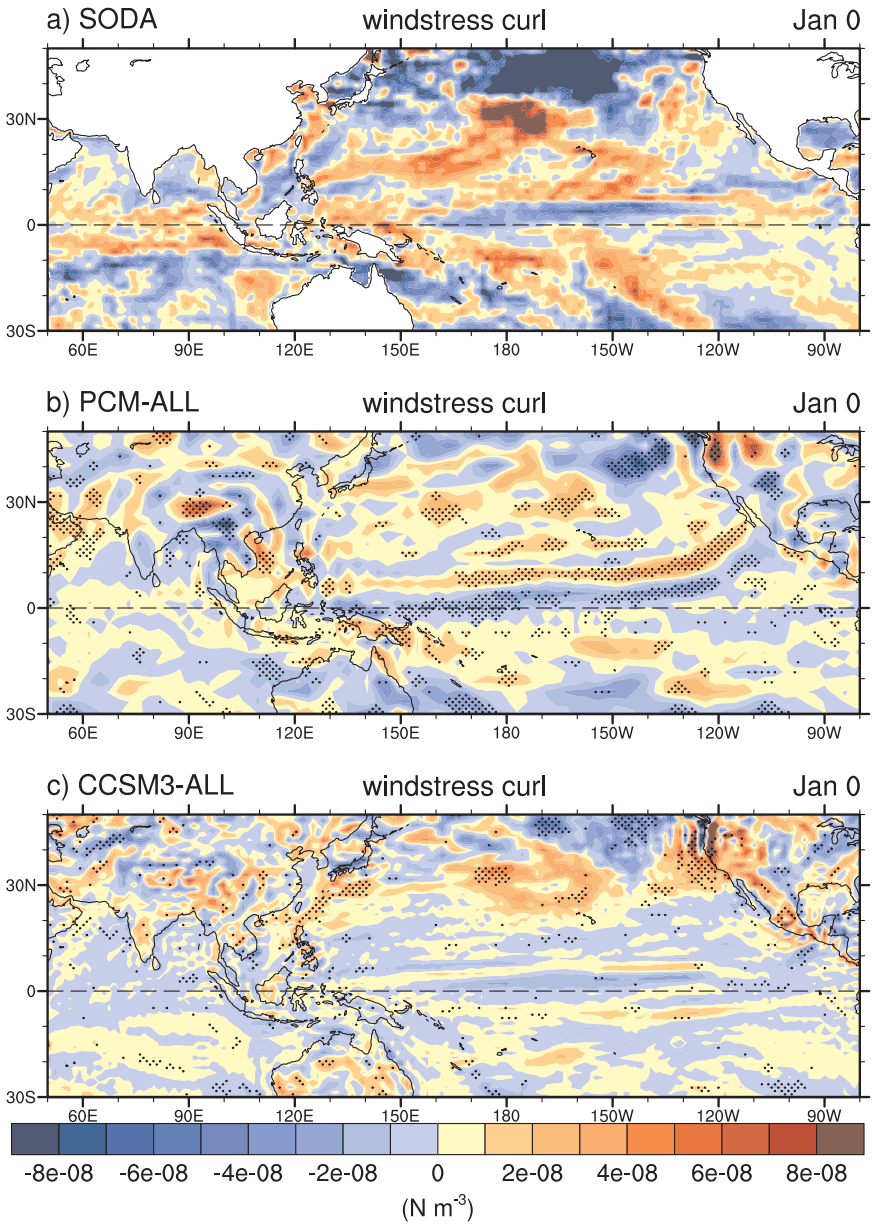

FIG. 8. (a) Composite wind stress curl differences from the SODA ocean reanalysis for January at the peak solar years, denoted as Jan 0. (b) As in (a), but for PCM Jan 0. (c) As in (a), but for CCSM3 Jan 0. Units are on the color bar and stippling indicates that the composite difference exceeds one interensemble standard deviation. The dashed line indicates the equator.

(Niño-3.4 = −0.06° and +0.17°C). Therefore, there is quantitative evidence from the observations and PCM (and a physically consistent response in CCSM3) to support the hypothesis that the negative value of Niño-3.4 at peak solar, followed by a positive value two years later, is significant in the observations and one of the models, with the other model having the correct sign sequence, indicating that solar forcing likely does force this particular interannnual response.

Clement et al. (1996) and Liu (1998) note that the response of the Pacific climate system to a uniform surface heat flux forcing across the equatorial Pacific could produce a cold event–like response. However, the solar forcing is not uniform, only affecting the surface where the sun is shining in relatively cloud-free areas (Meehl et al. 2003, 2008). Meehl et al. (2000) emphasize the importance of cloud feedbacks for the nonuniformity of radiative forcing and the SST response across

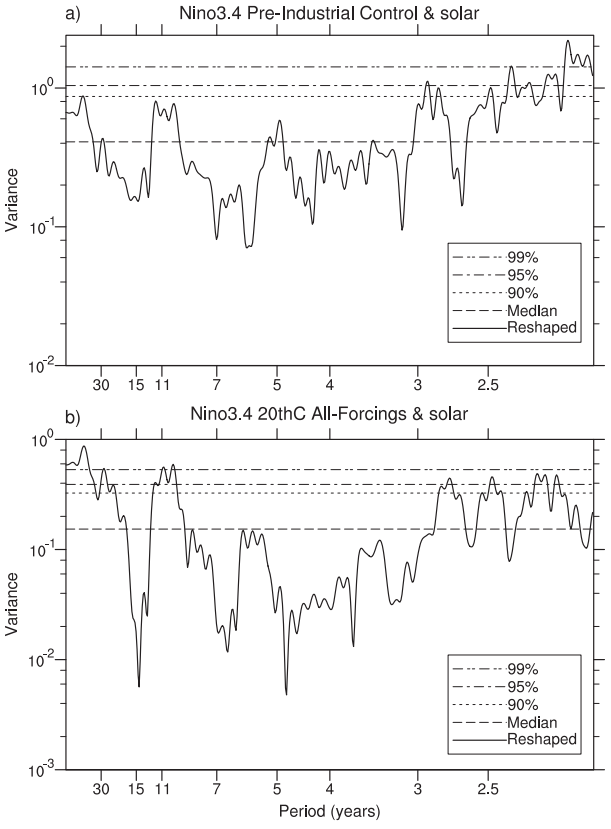

FIG. 9. Joint MTM/SVD spectra for Niño-3.4 and solar forcing from CCSM3 for the (a) preindustrial control run and (b) multimember ensemble average of twentieth-century all-forcings simulations, which include solar forcing. Significance levels are defined, and the solid line is the reshaped MTM-SVD spectra after the tapers are applied. Note the significant peak near 11 yr in (b) but not in (a), indicating that solar forcing near the 11-yr frequency forces a similar frequency response in Niño-3.4 SSTs in the model.

the equatorial Pacific. However, Liu (1998) points out the effects of off-equatorial heat flux forcing in the fast response of equatorial Pacific SSTs. Indeed, the relatively cloud-free subtropics play a crucial role in the coupled air–sea solar mechanism discussed in the present paper, and the processes described by Liu (1998) may be contributing to this response.

One could ask whether the tropical Pacific response documented in this paper is not just ENSO. In fact, the manifestation of ENSO could be influenced in ways postulated by White and Liu (2008b) as noted above. However, for the earlier work this paper builds on, van Loon et al. (2007) note that the composite signal for the tropical Pacific response to peaks in solar forcing in observations is similar if El Niño and La Niña events are omitted. Additionally, van Loon and Meehl (2008) show that the signature for ENSO and peak solar years is quite different in the stratosphere. By averaging over multiple ensemble members in the model simulations, most of the effects of individual ENSO events are removed, leaving the response to the peaks in the solar forcing in the models. Additionally, the forced Niño-3.4 signal compared to internally generated ENSO noise is significant for the observations and one of the models, as discussed above, thus quantifying the linkage between solar forcing and the response of Niño-3.4 SSTs.

Acknowledgments. The authors acknowledge Warren White, Zhengyu Liu, Yves Tourre, and Roland Madden for their helpful comments and discussions. Thanks to Gary Strand for helping with data processing. Portions of this study were supported by the Office of Science (BER), U.S. Department of Energy, Cooperative Agreement DE-FC02-97ER62402, and the National Science Foundation.

REFERENCES

Balachandran, N., D. Rind, P. Lonergan, and D. Shindell, 1999: Effects of solar cycle variability on the lower stratosphere and the troposphere. *J. Geophys. Res.,* **104,** 27 321–27 339.

Carton, J. A., G. Chepurin, X. H. Cao, and B. Giese, 2000: A simple ocean data assimilation analysis of the global upper ocean 1950–95. Part I: Methodology. *J. Phys. Oceanogr.,* **30,** 294–309.

Clement, A., R. Seager, M. A. Cane, and S. E. Zebiak, 1996: An oceanic dynamical thermostat. *J. Climate,* **9,** 2190–2196.

Collins, W. D., and Coauthors, 2006: The Community Climate System Model version 3 (CCSM3). *J. Climate,* **19,** 2122–2143.

Dai, A., T. M. L. Wigley, G. A. Meehl, and W. M. Washington, 2001: Effects of stabilizing atmospheric CO_2 on global climate in the next two centuries. *Geophys. Res. Lett.,* **28,** 4511–4514.

Deser, C., A. Capotondi, R. Saravanan, and A. S. Phillips, 2006: Tropical Pacific and Atlantic climate variability in CCSM3. *J. Climate,* **19,** 2451–2481.

Dettinger, M. D., M. Ghil, C. M. Strong, W. Weibel, and P. Yiou, 1995: Software expedites singular-spectrum analysis of noisy time series. *Eos, Trans. Amer. Geophys. Union,* **76,** 12–21.

Ghil, M., and Coauthors, 2002: Advanced spectral methods for climatic time series. *Rev. Geophys.,* **40,** 1003, doi:10.1029/2000RG000092.

Gleisner, H., and P. Thejll, 2003: Patterns of troposheric response to solar variability. *Geophys. Res. Lett.,* **30,** 1711, doi:10.1029/2003GL017129.

Haigh, J. D., 2001: Climate variability and the influence of the sun. *Science,* **294,** 2109–2111.

——, 2003: The effects of solar variability on the Earth's climate. *Philos. Trans. Roy. Soc. London,* **A361,** 95–111.

——, M. Blackburn, and R. Day, 2005: The response of tropospheric circulation to perturbations in lower-stratospheric temperature. *J. Climate,* **18,** 3672–3685.

Hoyt, D. V., and K. H. Schatten, 1993: A discussion of plausible solar irradiance variations, 1700–1992. *J. Geophys. Res.,* **98,** 18 895–18 906.

——, and ——, 1997: *The Role of the Sun in Climate Change*. Oxford University Press, 279 pp.

Kodera, K., 2004: Solar influence on the Indian Ocean Monsoon through dynamical processes. *Geophys. Res. Lett.,* **31,** L24209, doi:10.1029/2004GL020928.

Kuroda, Y., and K. Kodera, 2004: Role of the Polar-night Jet Oscillation on the formation of the Arctic Oscillation in the Northern Hemisphere winter. *J. Geophys. Res.,* **109,** D11112, doi:10.1029/2003JD004123.

Lean, J., and D. Rind, 2001: Earth's response to a variable sun. *Science,* **292,** 234–236.

——, J. Beer, and R. Bradley, 1995: Reconstruction of solar irradiance since 1610: Implications for climate change. *Geophys. Res. Lett.,* **22,** 3195–3198.

——, G. Rottman, J. Harder, and G. Kopp, 2005: SORCE contributions to new understanding of global change and solar variability. *Sol. Phys.,* **230,** 27–53.

Liu, Z., 1998: The role of ocean in the response of tropical climatology to global warming: The west–east SST contrast. *J. Climate,* **11,** 864–875.

Mann, M. E., and J. Park, 1999: Oscillatory spatio-temporal signal detection in climate studies: A multiple-taper spectral domain approach. *Advances in Geophysics,* Vol. 41, Academic Press, 1–131.

——, M. A. Cane, S. E. Zebiak, and A. Clement, 2005: Volcanic and solar forcing of the tropical Pacific over the past 1000 years. *J. Climate,* **18,** 447–456.

Matthes, K., Y. Kuroda, K. Kodera, and U. Langematz, 2006: Transfer of the solar signal from the stratosphere to the troposphere: Northern winter. *J. Geophys. Res.,* **111,** D06108, doi:10.1029/2005JD006283.

Meehl, G. A., 1987: The annual cycle and interannual variability in the tropical Pacific and Indian Ocean regions. *Mon. Wea. Rev.,* **115,** 27–50.

——, W. D. Collins, B. Boville, J. T. Kiehl, T. M. L. Wigley, and J. M. Arblaster, 2000: Response of the NCAR climate system model to increased CO_2 and the role of physical processes. *J. Climate,* **13,** 1879–1898.

——, P. Gent, J. M. Arblaster, B. Otto-Bliesner, E. Brady, and A. Craig, 2001: Factors that affect the amplitude of El Niño in global coupled climate models. *Climate Dyn.,* **17,** 515–526.

——, W. M. Washington, T. M. L. Wigley, J. M. Arblaster, and A. Dai, 2003: Solar and greenhouse gas forcing and climate response in the twentieth century. *J. Climate,* **16,** 426–444.

——, ——, C. Ammann, J. M. Arblaster, T. M. L. Wigley, and C. Tebaldi, 2004: Combinations of natural and anthropogenic forcings and twentieth-century climate. *J. Climate,* **17,** 3721–3727.

——, H. Teng, and G. W. Branstator, 2006a: Future changes of El Niño in two global coupled climate models. *Climate Dyn.,* **26,** 549–566.

——, and Coauthors, 2006b: Climate change projections in the twenty-first century and climate change commitment in the CCSM3. *J. Climate,* **19,** 2597–2616.

——, J. M. Arblaster, G. Branstator, and H. van Loon, 2008: A coupled air–sea response mechanism to solar forcing in the Pacific region. *J. Climate,* **21,** 2883–2897.

Rayner, N., D. Parker, E. Horton, C. Folland, L. Alexander, D. Rowell, E. Kent, and A. Kaplan, 2003: Global analyses of sea surface temperature, sea ice, and night marine air temperature since the late nineteenth century. *J. Geophys. Res.,* **108,** 4407, doi:10.1029/2002JD002670.

Rind, D., 2002: The sun's role in climate variations. *Science,* **296,** 673–677.

Shindell, D., D. Rind, N. Balachandran, J. Lean, and P. Lonergan, 1999: Solar cycle variability, ozone, and climate. *Science,* **284,** 305–308.

——, G. Faluvegi, R. L. Miller, G. A. Schmidt, J. E. Hansen, and S. Sun, 2006: Solar and anthropogenic forcing of tropical hydrology. *Geophys. Res. Lett.,* **33,** L24706, doi:10.1029/2006GL027468.

Tourre, Y. M., and W. B. White, 2006: Global climate signals and equatorial SST variability in the Indian, Pacific and Atlantic oceans during the 20th century. *Geophys. Res. Lett.,* **33,** L06716, doi:10.1029/2005GL025176.

van Loon, H., and K. Labitzke, 1994: The 10–12 year atmospheric oscillation. *Meteor. Z.,* **3,** 259–266.

——, and D. J. Shea, 2000: The global 11-year solar signal in July–August. *Geophys. Res. Lett.,* **27,** 2965–2968.

——, and G. A. Meehl, 2008: The response in the Pacific to the sun's decadal peaks and contrasts to cold events in the Southern Oscillation. *J. Atmos. Sol.-Terr. Phys.,* **70,** 1046–1055.

——, ——, and J. M. Arblaster, 2004: A decadal solar effect in the tropics in July–August. *J. Atmos. Sol.-Terr. Phys.,* **66,** 1767–1778.

——, ——, and D. J. Shea, 2007: Coupled air–sea response to solar forcing in the Pacific region during northern winter. *J. Geophys. Res.,* **112,** D02108, doi:10.1029/2006JD007378.

Washington, W. M., and Coauthors, 2000: Parallel climate model (PCM) control and transient simulations. *Climate Dyn.,* **16,** 755–774.

White, W. B., and Y. M. Tourre, 2003: Global SST/SLP waves during the 20th century. *Geophys. Res. Lett.,* **30,** 1651, doi:10.1029/2003GL017055.

——, and Z. Liu, 2008a: Resonant excitation of the quasi-decadal oscillation by the 11-year signal in the Sun's irradiance. *J. Geophys. Res.,* **113,** C01002, doi:10.1029/2006JC004057.

——, and ——, 2008b: Non-linear alignment of El Niño to the 11-yr solar cycle. *Geophys. Res. Lett.,* **35,** L19607, doi:10.1029/2008GL034831.

——, J. Lean, D. R. Cayan, and M. D. Dettinger, 1997: Response of global upper ocean temperature to changing solar irradiance. *J. Geophys. Res.,* **102,** 3255–3266.

——, M. D. Dettinger, and D. R. Cayan, 2003: Sources of global warming of the upper ocean on decadal period scales. *J. Geophys. Res.,* **108,** 3248, doi:10.1029/2002JC001396.